MECSOL 2019 - Proceedings of the 7th International Symposium on Solid Mechanics,
V. Tita, A. Ferreira, M.L. Ribeiro, A. Vieira and A.T. Beck (Editors), ABCM, Sao Carlos, SP, Brazil, April 15th to 17th, 2019

Longitudinal and Flexural wave modes interacting with an asymmetric corrosion-type fault on a beam

Camila Gianini Gonsalez Bueno, Michael John Brennan

São Paulo State University (UNESP), Department of Mechanical Engineering, Ilha Solteira, SP, Brazil.

Abstract: The development of systems for Structural Health Monitoring (SHM) has been desired by many researchers and companies around the world for many years. The techniques reported in the literature often involve the post processing of measured output signals after applying an excitation force on the structure. However, details of the physics behind the interaction of the elastic guided waves generated by these actuators and damage is not well understood. This paper discusses the interaction of elastic waves with an asymmetric fault similar to that due to corrosion. A state vector formulation is used to define relations between reflected and transmitted longitudinal and transversal waves on a beam. The proposed methodology allows the definition of the best frequencies to apply in the structural excitation. The results show some advantages of using the pulse-echo sensor configuration in comparison with pitch-catch one. Also, the longitudinal wave mode is shown to be better in the detection and quantification of corrosion faults.

Keywords: Longitudinal waves, Flexural waves, piezoelectric patches, Structural Health Monitoring, corrosion, SHM

INTRODUCTION

Several types of SHM systems have been proposed and developed in the past. In particular, guided wave-based techniques have received much attention because of their inherent advantages. To illustrate the advantages of such methods Mitra and Gopalakrishnan (2016) discussed the ability to scan a large area with a relatively small number of transducers. High frequency excitation is involved, meaning that small structural defects can be detected, and the transducers used are cheap, light-weight, and can be relatively easily incorporated into the structure. There are many studies showing aspects of using guided waves to detect fatigue cracks (Chan et al., 2015) and corrosion (Chew and Fromme, 2014).

Recently, Poddar and Giurgiutiu (2015) presented an analytical model for Lamb wave interaction with the simplest geometric discontinuity – a step (or asymmetric reduction of cross-sectional area), since this fundamental understanding can easily be extended to corrosion or a crack. The authors developed an analytical approach using the method called complex mode expansion with vector projection (CMEP) to predict the scatter of Lamb waves produced by the discontinuity.

Although many researchers have used guided wave-based approaches for SHM work, the physical mechanisms of wave scattering due to asymmetric damage is not well reported in the literature. This is the motivation for this work. This paper presents an investigation into the way in which longitudinal and flexural waves interact with an asymmetric corrosion-like fault, when symmetric piezoelectric actuators and sensors (PZTs – Lead zirconate titanate) are used to generate and measure wave scattering. The proposed approach offers promise for the development of SHM systems, because it can be a way to obtain an early prediction of a SHM system efficiency, reducing waste with validation tests such as Probability of Detection tests.

WAVE MODEL

Figure 1 shows the system of interest. It is an infinite beam with symmetric actuator and sensors consisting of PZT elements, and the asymmetric corrosion-like damage is located in the middle of the beam. The input voltage is applied to the actuator (PZTs 1) and measured at the sensors (PZTs 1 and PZTs 2).

The approach adopted in this work was previously presented and discussed by Brennan (1994), Brennan et al. (1997) and Ayala (2015). It involves the division of the beam shown in Fig.1 into segments. Euler-Bernoulli beam theory is

considered for the model, and the basic principle of the approach is to transform the waves at each end of a segment to a state vector, so that

$$\mathbf{h} = \mathbf{H}\mathbf{a} \tag{1}$$

where $\mathbf{h}$ is the state vector, $\mathbf{H}$ is the transformation matrix and $\mathbf{a}$ is the vector of wave amplitudes, which are respectively given by

$$\mathbf{h} = \{u \quad w \quad \theta \quad M \quad Q \quad F\}^T \tag{2}$$

where u is the axial displacement, w is transversal displacement, θ is the slope, M is the moment, Q is the shear force and F is axial force,

$$\mathbf{H} = \begin{bmatrix} 0 & 0 & 1 & 0 & 0 & 1 \\ 1 & 1 & 0 & 1 & 1 & 0 \\ k_f & jk_f & 0 & -k_f & -jk_f & 0 \\ E_b I_b k_f^2 & -E_b I_b k_f^2 & 0 & E_b I_b k_f^2 & -E_b I_b k_f^2 & 0 \\ E_b I_b k_f^3 & -jE_b I_b k_f^3 & 0 & -E_b I_b k_f^3 & jE_b I_b k_f^3 & 0 \\ 0 & 0 & jE_b S_b k_l & 0 & 0 & -jE_b S_b k_l \end{bmatrix} \tag{3}$$

where E_b is the Young's modulus of the beam, I_b is the second moment of area of beam, S_b is the cross-sectional area of the beam, $j = \sqrt{-1}$, k_l is the longitudinal wavenumber and k_f is the flexural wavenumber, and

$$\mathbf{a} = \{A_1 \quad A_3 \quad A_l \quad A_2 \quad A_4 \quad A_r\}^T \tag{4}$$

where (for a horizontal beam) A_1 is the amplitude of a left-going near-field wave, A_3 is the amplitude of a left-going propagating wave, A_l is the amplitude of left-going longitudinal wave, A_2 is the amplitude of a right-going near-field, A_4 is the amplitude of a right-going propagating wave, and A_r is the amplitude of a right-going longitudinal wave.

Figure 1 – Segments of the system studied (infinite beam).

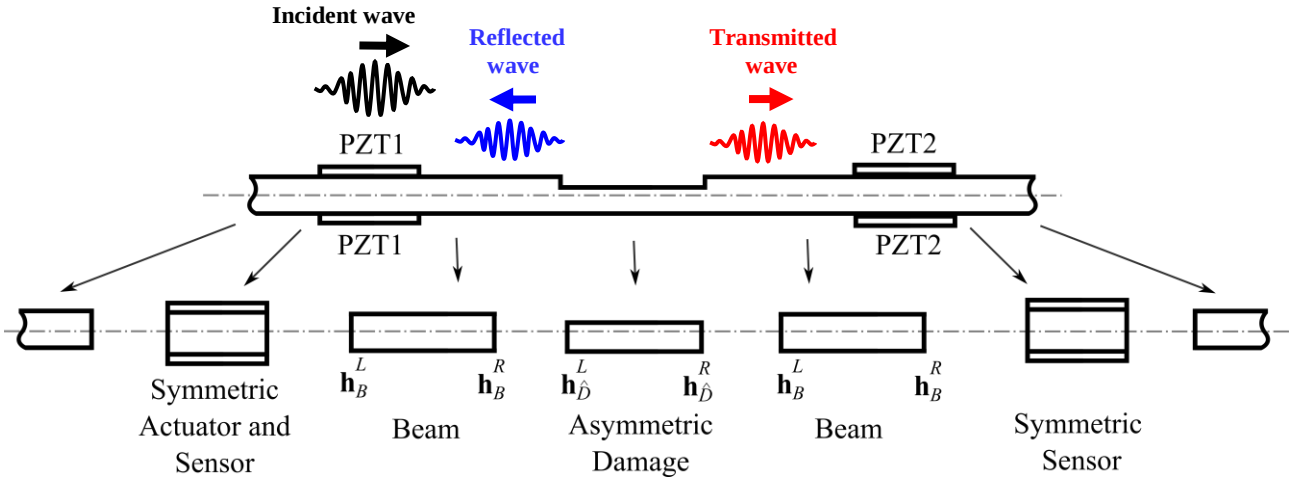

Figure 1 also illustrates two configurations usually used for detecting damage. In the pulse echo configuration when piezoelectric elements PZT1 are used as both actuator and sensor to detect the reflected waves from the damage (blue wave packet). In the pitch-catch configuration the piezoelectric elements PZT1 are used as the actuator and PZT2 are used as sensor to detect the waves transmitted past the damage.

Beam segment

The system studied is divided into segments and the state vectors of the connections at each end of a beam segment are given by

$$\mathbf{h}_B^L = \mathbf{H}_B \mathbf{a}_B^L \qquad \mathbf{h}_B^R = \mathbf{H}_B \mathbf{a}_B^R \tag{5,6}$$

where the subscript B indicates that the variable belongs to the beam without damage and the superscripts L and R denote the left- and right-hand junctions of the segment. The relationship between the wave vectors $\mathbf{a}_B^L$ and $\mathbf{a}_B^R$ is given by

$$\mathbf{a}_B^R = \mathbf{T}_B \mathbf{a}_B^L \tag{5}$$

where $\mathbf{T}_B$ is the wave transmission matrix for a segment of the beam, given by

$$\mathbf{T}_B = diag\left(e^{k_f l_B}, e^{jk_f l_B}, e^{jk_l l_B}, e^{-k_f l_B}, e^{-jk_f l_B}, e^{-jk_l l_B}\right) \tag{6}$$

where $diag$ indicates a diagonal matrix, and l_B is the length of the segment.

Piezoelectric actuator

A symmetric or two-element piezoelectric actuator (piezoelectric elements fitted to opposite sides of the beam) can generate longitudinal and flexural waves separately in a beam depending on the relative phase of the voltage supply to the piezoelectric patches. Figure 2 shows the waves types generated.

Figure 2 – Symmetric piezoelectric actuators; (a) longitudinal waves generated by a pair of forces and (b) transversal waves generated by a pair of moments.

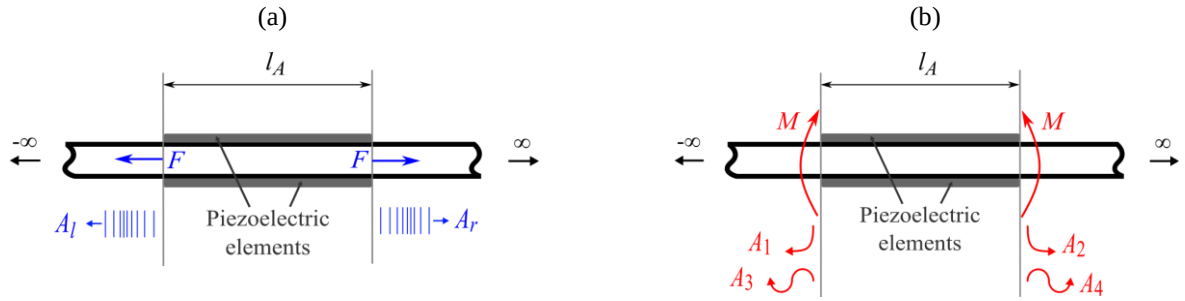

The amplitudes of waves generated by a pair of forces F and a pair of moments M are given by (Brennan, 1994) as

$$\begin{Bmatrix} A_l \\ A_r \end{Bmatrix} = \frac{-j}{2k_l E_b S_b} \begin{bmatrix} 1 & e^{-jk_l l_A} \\ 1 & e^{jk_l l_A} \end{bmatrix} \begin{Bmatrix} -F \\ F \end{Bmatrix}, \qquad \begin{Bmatrix} A_1 \\ A_2 \\ A_3 \\ A_4 \end{Bmatrix} = \frac{1}{4k_f^2 E_b I_b} \begin{bmatrix} 1 & e^{-k_f l_A} \\ -1 & -e^{k_f l_A} \\ -1 & -e^{-k_f l_A} \\ 1 & e^{jk_f l_A} \end{bmatrix} \begin{Bmatrix} M \\ -M \end{Bmatrix} \tag{9,10}$$

where l_A is the length of the PZT actuator. The power in the longitudinal and flexural propagating right going waves are respectively given by (Brennan et al., 1997)

$$P_l = (1/2) E_b S_b k_l \omega |A_r|^2, \qquad P_f = E_b I_b k_f^3 \omega |A_4|^2 \tag{11,12}$$

To study the wave interactions with the asymmetric damage in an infinite beam with symmetric actuators as shown in Figure 1, the properties of the beam and the piezoelectric patches are chosen as in Table 1.

Table 1 – Geometrical and material properties of infinite beam and piezoelectric elements

Properties	Piezoelectric elements	Beam
Material	PSI-5H4E	Al (6063-T5)
Young's Modulus [N/m²]	62×10^9	68.9×10^9
Density [kg/m³]	7800	2700
Relative Dielectric Constant	3800	--
Piezoelectric Coefficient [m/V] or [C/N]	-320×10^{-12}	--
Width [m]	12.7×10^{-3}	12.7×10^{-3}
Depth [m]	2.67×10^{-4}	1.58×10^{-3}

Using Equations (9) and (10), the amplitudes of the outgoing right-going propagating waves generated by the actuator per unit force and moment respectively, are calculated and are plotted in Figure 3. These waves will interact with the damaged section. The graphs in Figure 3 are plotted in terms of frequency and the non-dimensional parameter of wavelength and actuator length. In Figure 3(a), λ_l is the longitudinal wavelength and in Figure 3(b) λ_f is the flexural wavelength. The square of the latter is plotted to obtain a linear relationship with frequency.

Figure 3 – Amplitude of right-going waves from symmetric actuator of length $l_A = 0.0127m$; (a) longitudinal waves and; (b) flexural propagating waves.

(a) (b)

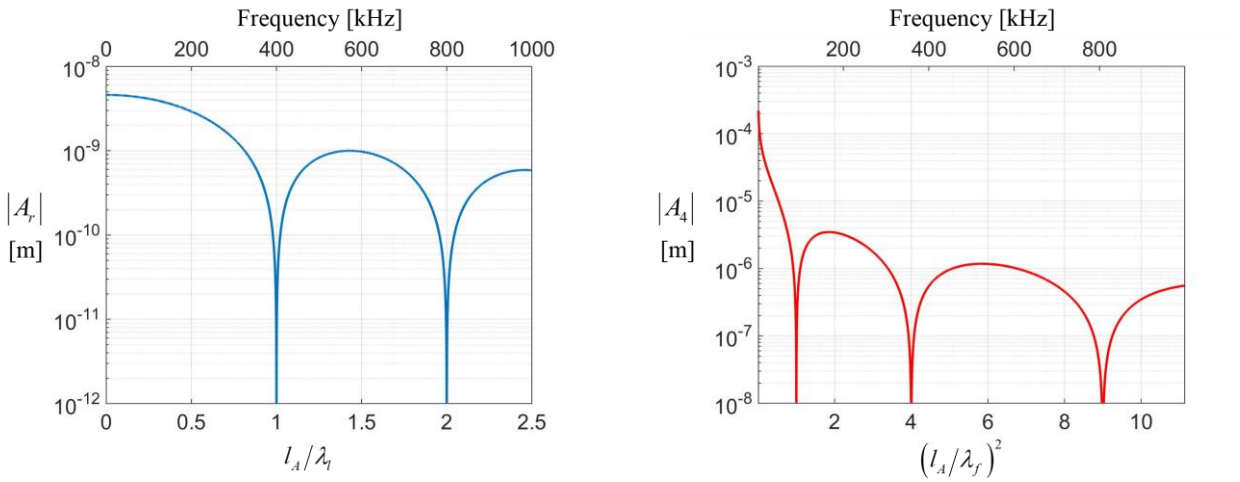

It is possible to observe the filtering effects of the actuators in Figures 3(a) and (b), When the wavelength of the respective waves is an integer multiple of the actuator size, such that

$$l_A/\lambda_l = l_A/\lambda_f = 1,2,...,n \in \mathbb{N} \tag{7}$$

no propagating waves are generated by the actuator. In the design of an SHM system it is important to avoid these frequencies.

Asymmetric damage

Due to the asymmetry of the area change as a result of the corrosion damage, an additional moment, which is proportional to the distance between the neutral axis of the beam segment and the segment representing the damage, is generated. This is illustrated in Figure 4.

Figure 4 – Junctions between the asymmetric damage and adjacent beams segments.

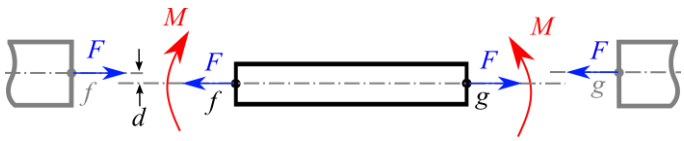

In this case, the state vector at the junctions has to be modified, so that

$$\mathbf{h}_{\hat{D}} = \mathbf{h}_D + \mathbf{h}_{Asym} \tag{8}$$

where $\mathbf{h}_{\hat{D}}$ is the state vector of asymmetric damaged section, $\mathbf{h}_D$ is the state vector for a symmetric damaged section of beam, and $\mathbf{h}_{Asym}$ is at the junction between them, given by

$$\mathbf{h}_{Asym} = \{-\theta d \quad 0 \quad 0 \quad Fd \quad 0 \quad 0\}^T \tag{9}$$

It is possible to write down an expression relating the incoming and outgoing waves to and from the damaged section. It is given by

$$\boldsymbol{\gamma}\mathbf{a}_{\mathbf{o}} + \boldsymbol{\mu}\mathbf{a}_{\mathbf{i}} = \mathbf{0} \tag{10}$$

where $\mathbf{a}_{\mathbf{o}}$ is the vector of outgoing waves amplitudes (reflected and transmitted), the $\mathbf{a}_{\mathbf{i}}$ is the vector of incoming wave amplitudes (incident), given by

$$\mathbf{a}_{\mathbf{o}} = \{A_{1B} \quad A_{3B} \quad A_{lB} \quad A_{2D} \quad A_{4D} \quad A_{rD}\}^T \tag{11}$$

$$\mathbf{a}_{\mathbf{i}} = \{A_{1D} \quad A_{3D} \quad A_{lD} \quad A_{2B} \quad A_{4B} \quad A_{rB}\}^T \tag{12}$$

where the superscript D is related with the damage segment. After some re-arrangement, the matrices $\boldsymbol{\gamma}$ and $\boldsymbol{\mu}$ can be determined, and are given by

$$\boldsymbol{\gamma} = [\boldsymbol{\gamma}_1 \quad \boldsymbol{\gamma}_2 \quad \boldsymbol{\gamma}_3 \quad \boldsymbol{\gamma}_4 \quad \boldsymbol{\gamma}_5 \quad \boldsymbol{\gamma}_6]$$
$$\text{where } \boldsymbol{\gamma}_i = \left(-\mathbf{H}_{\hat{D}}\mathbf{T}_{\hat{D}}\mathbf{H}_{\hat{D}}^{-1}\mathbf{H}_B\right)_i \qquad i = 1,2,3, \quad \text{and} \quad \boldsymbol{\gamma}_i = \left(\mathbf{H}_B\right)_i \qquad i = 4,5,6 \tag{13}$$

and

$$\boldsymbol{\mu} = [\boldsymbol{\mu}_1 \quad \boldsymbol{\mu}_2 \quad \boldsymbol{\mu}_3 \quad \boldsymbol{\mu}_4 \quad \boldsymbol{\mu}_5 \quad \boldsymbol{\mu}_6]$$
$$\text{where } \boldsymbol{\mu}_i = \left(\mathbf{H}_B\right)_i \qquad i = 1,2,3, \quad \text{and} \quad \boldsymbol{\mu}_i = \left(-\mathbf{H}_{\hat{D}}\mathbf{T}_{\hat{D}}\mathbf{H}_{\hat{D}}^{-1}\mathbf{H}_B\right)_i \qquad i = 4,5,6 \tag{14}$$

When a longitudinal wave is incident on the asymmetric damage section it scatters into reflected and transmitted longitudinal waves and reflected and transmitted flexural waves, as shown in Figure 5(a). The same occurs for an incident flexural wave, as shown in Figure 5(b).

Figure 5 – Scattering waves by an asymmetric damage for incident; (a) Longitudinal wave and; (b) Flexural wave

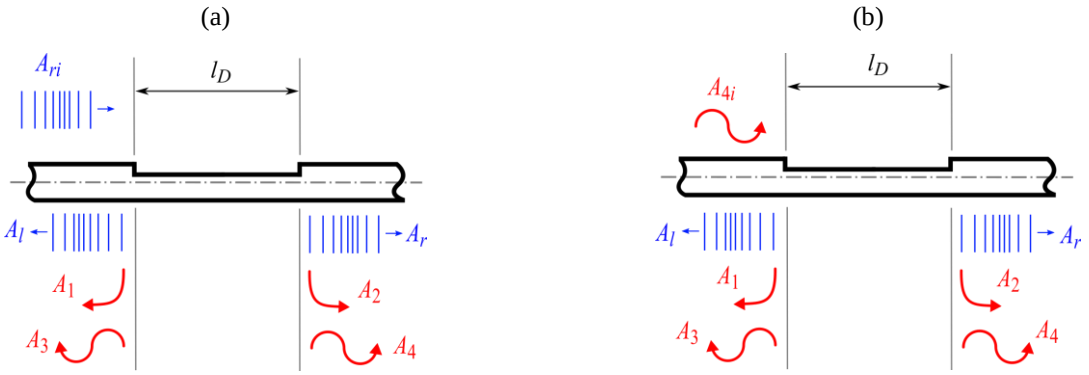

Using the modelling approach described above, the waves scattered by the damaged section can be calculated and are shown in Figures 6 and 7. The damaged section is $0.025m$ long, and three levels of damage are considered, so that the reduction in the beam thickness is 10, 30 and 50%. In Figures 6(a) and 7(a) an incident longitudinal wave is considered and in Figures 6(b) and 7(b) an incident flexural wave is considered.

Examining Figure 6 and 7, the filtering effects of the damage can be seen at certain frequencies when an incident wave passes through the damage without being affected. This means that at these frequencies the waves are not able to detect the damage. Thus, in an SHM system, frequency ranges close to these frequencies must be avoided.

In Figure 6 it is clear that the longitudinal reflected waves are more sensitive to the damage than longitudinal transmitted and flexural reflected and transmitted waves. Thus it is recommended that this wave mode is used to detect and quantify a corrosion defect.

In Figure 7, when flexural waves are used, it is important to note that the filtering effects occur at different frequencies depending of the degree of damage. This is because they are dispersive, which is not the case with longitudinal waves. The highlighted region (between 40 and 60 kHz) represents the frequency range in which the beam is excited in the section on the Complete System later in the paper.

Figure 6: Scattering waves in asymmetric damage with $l_D = 0.025m$ for an Incident longitudinal wave; (a) Scattered longitudinal waves; (b) Scattered flexural waves.

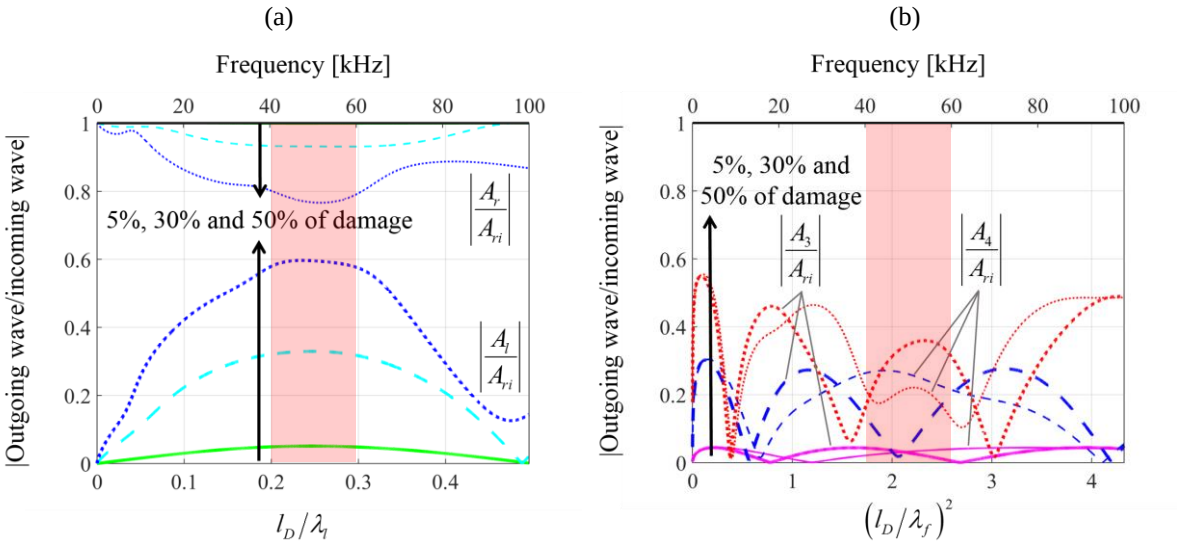

Figure 7: Scattering waves in asymmetric damage with $l_D = 0.025m$ for an incident flexural wave; (a) Scattered longitudinal waves; (b) Scattered flexural waves.

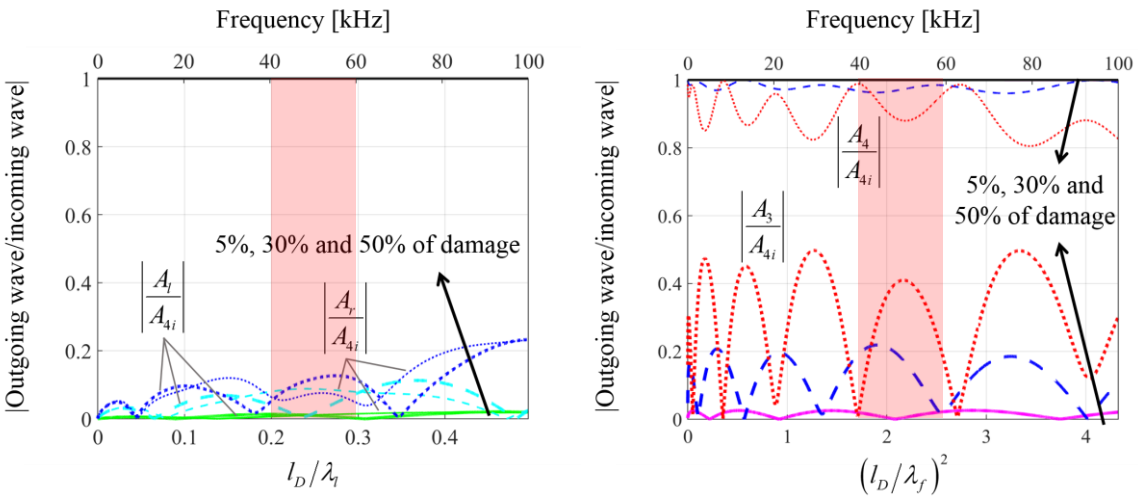

Piezoelectric sensor

As presented by Brennan (1994), piezoelectric patches can be coupled to a beam and configured to measure strain spatially integrated over the area they occupy. Figure 8 shows a schamtic diagram of the symmetric sensor used.

Figure 8: Piezoelectric sensor.

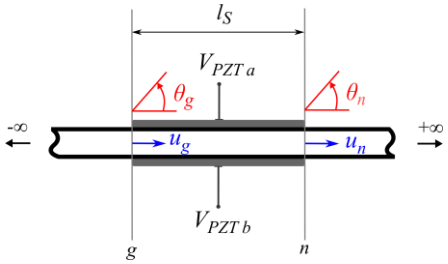

The simplified model of a sensor adopted here assumes that the PZT sensor elements have negligible mass and stiffness, and also the strain is constant across the width of the beam and the PZT elements. A longitudinal wave generates electrical voltage due to axis displacement, and is given by (Brennan, 1994)

$$V_l = \frac{d_{31} E_p b}{C_p}\left(u_n - u_g\right) \tag{15}$$

where d_{31}, b and C_p are respectively piezoelectric coefficient, width and capacitance of piezoelectric elements; u is the axial displacement, which is the sum of the left and right-going longitudinal waves, so that

$$u = A_l + A_r \tag{16}$$

and for each sensor extremity $u_g = A_{lg} + A_{rg}$ and $u_n = A_{ln} + A_{rn}$. A flexural wave generates electrical voltage due to the difference of the slopes at the ends of the sensor, and is given by (Brennan, 1994):

$$V_f = \frac{d_{31} w_p E_p b}{C_p}\left(\theta_n - \theta_g\right) \tag{17}$$

where $w_p = t_b/2 + t_p$ and θ is the slope given by:

$$\theta = k_f A_1 + jk_f A_2 - k_f A_3 - jk_f A_4 \tag{18}$$

and for each sensor extremity $\theta_g = k_f A_{1g} + jk_f A_{2g} - k_f A_{3g} - jk_f A_{4g}$ and $\theta_n = k_f A_{1n} + jk_f A_{2n} - k_f A_{3n} - jk_f A_{4n}$.

The filtering effect described for the actuator in Figure 3 also occurs for the sensor. In the work presented here, the piezoelectric patches for the actuator and sensor are the same size, so the frequencies to be avoided for the filtering effect of sensor and the actuator are the same.

Complete System

Figure 1 illustrates the complete assembled system. It is modeled in the frequency domain using the methodology presented above and transformed to the time domain using the Inverse Fast Fourier Transform (IFFT) (Oppenheim and Willsky, 2010).

To study the time responses for the system, an excitation signal with a centre frequency of 50kHz and a burst of five periods windowed by the Hanning window is chosen. This frequency is highlighted in Figures 6 and 7. Figure 9 illustrates this signal in the time and frequency domains. Figure 10 shows the scattered waves in the time domain for a longitudinal wave generated by the actuator, and Figure 11 shows the corresponding plots for flexural waves generated by the actuator.

From Figures 10 and 11 is possible to identify the longitudinal and the flexural wave packets. Note the non-dispersive behavior of the longitudinal waves (the waves that arrive first), and the dispersive behavior of the flexural waves (the waves that arrive second).

The behavior seen in Figures 10 and 11 correspond to the transmitted and reflected waves within the frequency range highlighted in Figures 6 and 7. Figure 10(a) shows clearly that reflected waves (longitudinal and flexural) are more sensitive to the damage compared with the transmitted waves shown in Fig. 10b. Also, it is interesting to note that the amplitude of the transmitted flexural waves for 50% reduction in beam thickness is almost the same for 30% reduction in beam thickness. Additionaly, the amplitude of the reflected flexural waves for 30% reduction in beam thickness is almost zero. It can thus be concluded that a simple comparision of flexural wave amplitudes is not enough to quantify the severity of damage. However, it can be seen that the longitudinal reflected wave amplitude can be used to detect and quantify the damage.

Figure 9: Input signal in; (a) time domain and; (b) frequency domain.

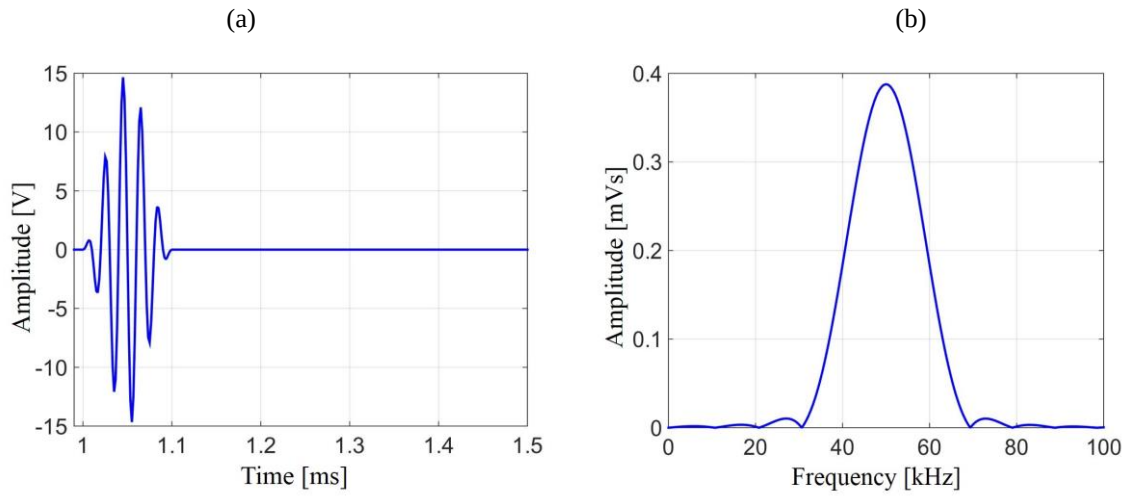

Figure 10: Scattered waves in asymmetric damage with $l_D = 0.025m$ for incident longitudinal waves; (a) reflected waves; (b) transmitted waves.

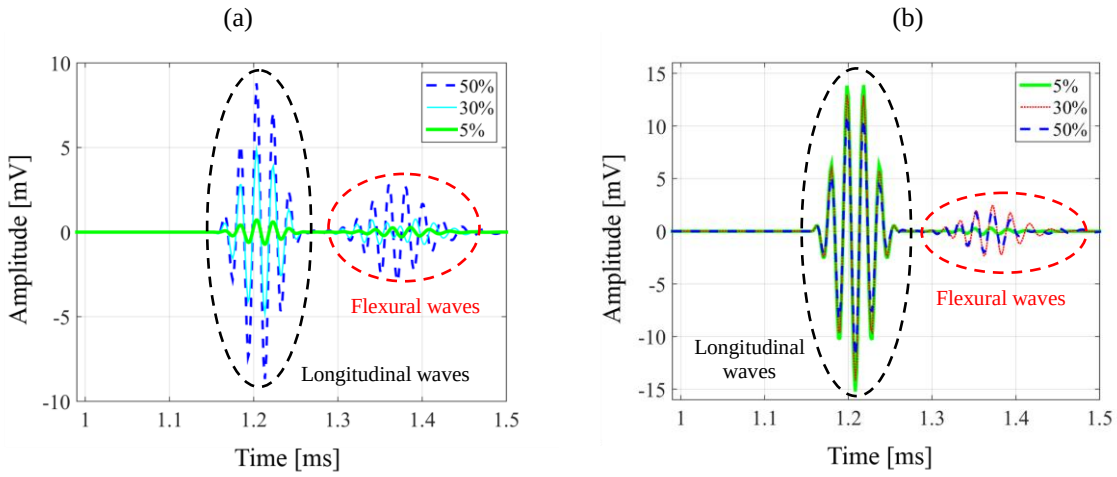

Figure 11a shows that the reflected flexural waves are more sensitive to damage severity. However, there is similar sensitivity for longitudinal transmitted and reflected waves, as shown in Figure 11(a) and (b). The longitudinal reflected waves are not propotional to the damage severity. It means that for flexural incident waves (50kHz range) it is recommended to use flexural reflected waves to detect and quantify the damage in the range studied here. However, the transmitted waves (longitudinal and flexural) can also be used to detect and quantify the damage.

Figure 11: Scattering waves in asymmetric damage with $l_D = 0.025m$ for incident flexural waves; (a) reflected waves; (b) transmitted waves.

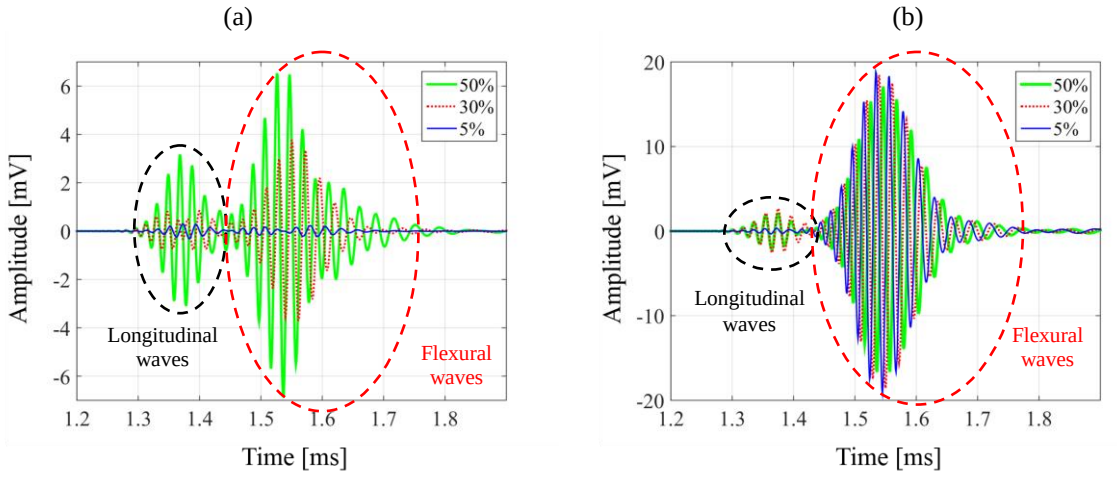

CONCLUSIONS

A study of wave interaction with asymmetric corrosion-type fault on a beam has been studied in this paper. To generate and sense waves PZT elements of same size used as actuator and sensor. A model of the system has been formulated in the frequency domain and then transformed to the time domain to perform simulations which are similar to experiments conducted in the laboratory. The frequency domain model has been used to demonstrate the wave filtering effects of the actuators, sensors and damage. The investigation has shown that, for SHM there are thus good and bad frequency ranges to apply the structural excitation. The time domain simulations which involve either a longitudinal or flexural wave packet being excited show that for a longitudinal wave packet incident on the damage, the highest sensitivity is for longitudinal reflected waves. Furthermore it has been shown that reflected flexural waves are more sensitive to damage severity when the incident wave is flexural. A general conclusion for the system studied is that a pulse-echo sensor configuration in better to detect the damage compared to a pitch-catch configuration considering the excited frequency range (50kHz).

ACKNOWLEDGMENTS

The authors are grateful the financial support provided by Coordination for the Improvement of Higher Education Personnel (CAPES). The first author would like to thanks Dr. Douglas Domingues Bueno and Msc. Pedro Christian Ayala Castilho for discussions and contributions on this research.

REFERENCES

Ayala, P. C., Detecção de danos em estruturas guiadas usando ondas de alta frequência, UNESP São Paulo State University - Faculty of Engineering of Ilha Solteira, 2015, 83p. Master's thesis.

Brennan, M. J., Active control of waves on one-dimensional structures, Faculty of Engineering and Applied Science, Institute of Sound and Vibration Research - ISVR, University of Southampton, 1994, PhD thesis.

Brennan, M. J., Elliott, S. J. and Pinnington, R. J., The dynamic coupling between piezoceramic actuators and a beam, *Journal of the Acoustical Society of America*, 1997, **102**(4), 1931–1942.

Chan, H., Masserey, B. and Fromme, P., High frequency guided ultrasonic waves for hidden fatigue crack growth monitoring in multi-layer model aerospace structures, *Smart Materials and Structures*, (24), 1–10, 2015

Chew, D. and Fromme, P., Monitoring of corrosion damage using high-frequency guided ultrasonic waves, *Proc. SPIE 9064, Health Monitoring of Structural and Biological Systems 2014*, 90642F (March 9, 2014), San Diego, California, USA, 2014.

Mitra, M. and Gopalakrishnan, S., Guided wave based structural health monitoring: A review, Smart Materials and Structures, 25 (5), 053001 (27pp), 2016.

Oppenheim, A. V. and Willsky, A. S., Sinais e Sistemas, Pearson, 2010.

Poddar, B. and Giurgiutiu, V., Poddar, B.; Giurgiutiu, V., Experimental Validation of Analytical Model for Lamb Wave Interaction with Geometric Discontinuity**,** *2015 Smart Structures and NDE*, San Diego, CA, 94371Y 9437-69, 8-12 March 2015.

RESPONSIBILITY NOTICE

The authors are the only responsible for the printed material included in this paper.